Experiments of convective evaporation of refrigerant R513A in a horizontal stainless-steel tube

Experiments of convective evaporation of refrigerant R513A in a horizontal stainless-steel tube

A Arcasi[1], R Mastrullo[1], A W Mauro[1*], A F Passarelli and I Viscardi[1]

[1] Department of Industrial Engineering, Federico II University of Naples, P.le Tecchio 80, 80125 Naples (Italy)
*Corresponding author e-mail: wmauro@unina.it

Abstract. Refrigerant R513A represents an interesting solution for the retrofit of conventional high-GWP fluorinated gases, such as R134a, R401A, R401B and R409A for low and medium temperature applications. R513A is an azeotropic mixture (almost zero-temperature glide at any operating pressure) made up of R134a and R1234yf (44% and 56% in mass, respectively), allowing at the same time a very low GWP of 580 and favourable safety characteristics such as no flammability and no toxicity (A1 ASHRAE class). The boiling performance of this blend is scarcely explored and studied in scientific literature, especially in case of commercial tubes typically adopted for refrigeration purposes. For this reason, this paper presents two-phase flow boiling experiments of refrigerant R513A in a 6.00 mm horizontal stainless-steel tube. Heat is provided by means of Joule effect directly on the tube surface, and the peripheral average heat transfer coefficients are obtained by measuring the temperatures at four sides (top, bottom, left and right) of the channel. The effect of the operating conditions is experimented and discussed, by varying the mass flux between 150 and 300 kg/m^2 s, saturation temperature between 20 and 50°C and imposed heat flux between 5 and 20 kW/m^2. Also, a comparison with the boiling performance of refrigerant R134a is proposed within the same operating conditions. Finally, the assessment of well-known flow boiling prediction methods is presented and discussed.

Keywords: *R513A; flow boiling, heat transfer coefficient, correlation assessment*

1. Introduction

In the last decades, the global warming issue has become of primary importance and several regulations have been involved to limit the impact of the anthropogenic activities on Earth's temperature increase. Among them, the Kigali Amendment to the Montreal Protocol [1] promoted the phase-out of the hydrofluorocarbon refrigerants (HFCs) and the European F-GAS regulation [2] restricted the use of high-GWP (Global Warming Potential) fluorinated gases in several applications, thus leading to their replacement. In this context, R134a refrigerant (GWP value of 1430) has to be substituted with new low-GWP mixtures such as R1234yf, R1234ze and R513A for medium temperatures and other blends like R452A, R455A and R448A for low temperature applications. On this regard, Citarella et al. [3] proposed a thermo-economic analysis to explore possible design options for a 2.5 kW commercial refrigeration unit by using several mixtures (R454C, R449A, R452A and R455A), finding that R454C could be a suitable alternative as long-term replacement for these applications. Sanchéz et al [3] experimentally studied the energy performance of a cooler using R290 as an alternative of R134a and found that propane reduce energy about 27.5% compared to the one of R134a. Zheng et al [5] compared the performance of R290 and R134a in a cool storage air conditioning system and found that the system COP was comparable to the one of R134a whereas the R290 system had a higher volumetric

refrigerating capacity. Mota-Babiloni et al. [6][7] experimentally analyzed the influence of using R134a and R513A refrigerants in a vapor compression system by varying evaporating and condensing conditions: it was found that R513A refrigerant leads both to a higher cooling capacity and COP values compared to the ones of R134a. The same considerations have been conducted by Zhang et al [8] and Sun et al [9]. New data on the two-phase heat transfer performance of these blends are particularly useful to test the accuracy of existing prediction methods for the correct design of condenser and evaporators employed in refrigeration systems. A literature review has pointed out numerous experimental studies on boiling of new R134a possible substitutes, either including pure fluids as R1234yf and R1234ze in conventional [10] and mini-channels [11], or non-azeotropic blends related to lower temperature applications, such as R452A [12], R455A [13] and R448A [14]. As regards instead the boiling performance of R513A, to the best of the authors' knowledge, the existing literature on this topic is scarce and limited to narrow diameter tubes. Diani et al [15][16] investigated both flow boiling and pressure drop performance of R513A in a 2.5 mm smooth and microfin tube comparing experimental results with the common predictive methods available in literature. In this study, experimental data of R513A during flow boiling in a 6.00 mm horizontal stainless-steel tube are collected. The effect of the operating parameters on the heat transfer coefficient in terms of saturation temperature, mass flux and heat flux are evaluated and discussed, by varying the saturation temperature between 20 and 50 °C, mass flux between 150 and 300 kg/m^2 s and heat flux between 5 and 20 kW/m^2. Finally, heat transfer comparison with the reference fluid R134a in the same operating conditions is investigated and the assessment of the well-known heat transfer coefficient correlations is proposed.

2. Experimental setup

2.1. Refrigerant and water loops

Figure 1 provides a photograph and a schematic representation of the experimental rig used in this paper. It consists of two different closed loops, one for the working fluid object of the study and one for the demineralized cooling water. In the refrigerant loop (black line) the employed fluid is pumped by a gear pump and goes into a Corolis mass flow meter. Then it passes into a preheating section whose heat capacity is about 3.6 kW and where it partially evaporates, achieving the desired vapor quality value. Successively it goes through the test section where the measurement of the heat transfer coefficient is attained. Finally, the saturated fluid reaches a plate condenser and a sub-cooler, before closing the loop. The demineralized cooling water loop (blue line) consists of a circulation pump and it feeds the sub-cooler and the condenser before going into the thermostatic bath, which controls its thermal level. More details of the whole experimental apparatus can be found in previous publications of the same authors [13][17]. The whole test bench is covered with several layers of synthetic foam to minimize the heat to and from the environment.

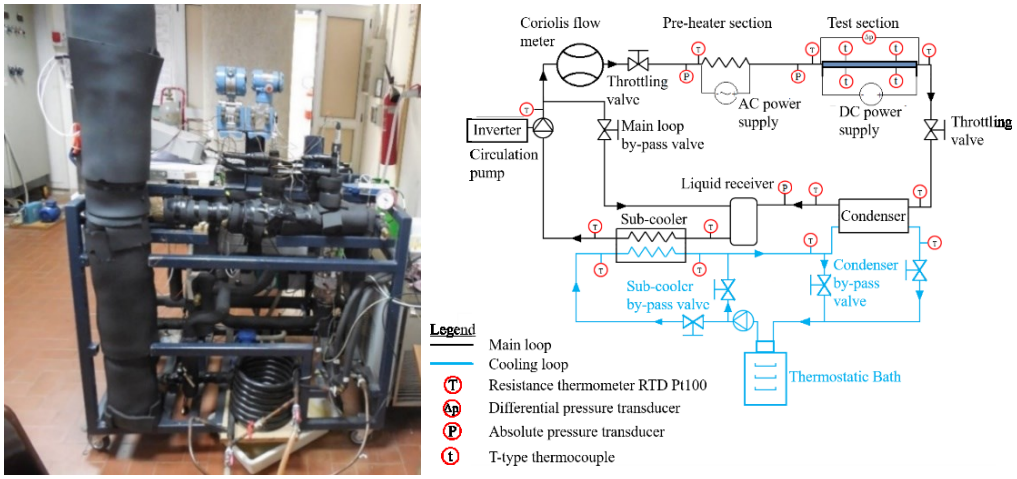

Figure 1. Photograph and representation of the experimental rig.

2.2. Test section and measurement instrumentation

All tests were performed in a single smooth horizontal stainless steel tube (AISI SS316) whose inner and outer diameters are 6.0 ±0.05 mm and 8.0 ±0.05 mm, respectively. All the geometrical features and characteristics of the test section are shown in Figure 2. Heat is provided by means of Joule effect directly on the tube surface with a DC power supply unit and two copper electrodes welded on the surface at a distance of 193.7 ±0.79 mm. Two wires are clamped in B and D position for the evaluation of the heat flux imposed. Four T-type thermocouples are placed on the external surface of the tube (point C) in the top, bottom, left and right position in order to evaluate the outer temperature distribution of the tube. The list of the measurement sensors and transducers employed in the experimental campaign is reported in Table 1 with their operative range and instrumental accuracy.

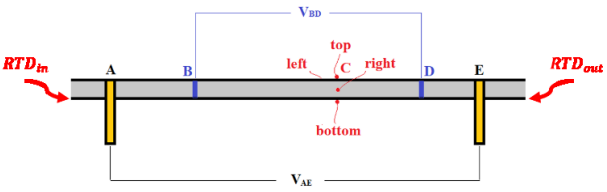

Geometrical features	
A,E	copper electrodes
B,D	voltage measurement points
C	temperature measurement point
AE	193.7 ±0.79 mm
BD	101.6 ±0.41 mm
AC	146.7 ±0.64 mm
d	6.00 ±0.05 mm (internal diameter)
D	8.00 ±0.05 mm (outer diameter)

Figure 2. Schematization and main geometrical characteristics of the test section.

Table 1. Specifications of the transducers and sensors with their operative range and accuracy.

Measurement	Range	Instrument accuracy
Temperature (4-wire Pt100 RTDs)	-80/250 °C	±0.180 °C
Wall temperature (T-type thermocouples)	10/90 °C	±0.1 °C
Inlet absolute pressure transducer (test section)	0/35 bar	±0.1% reading
Absolute pressure transducer (test rig)	0/50 bar	±0.3% reading
Differential pressure (test section)	0/14.51 kPa	±0.06 kPa
Coriolis flow meter $\dot{m}$	2.3/115.7 g/s	±1.0% reading
Electric power (pre-heater section)	0/3.6 kW	±1.0% reading
Voltage (test section) V_{BD}	0/5 V	±0.03% reading
Current (test section) I_{tube}	0/300 A	±1% reading

3. Method

3.1. Data reduction

The average heat transfer coefficient for each point is evaluated by the Newton equation with the assumption of uniform heat flux q and by considering the average wall temperature $T_{wall,mean}$ from the four T-type thermocouples measurements $T_{wall,o}$, as shown in Equation (1):

$$h_{mean} = \frac{q}{T_{wall,mean} - T_{sat,C}} \tag{1}$$

where the average wall temperature and the uniform heat flux are given by equations (2) and (3):

$$T_{wall,mean} = \frac{T_{wall,top} + T_{wall,bot} + T_{wall,left} + T_{wall,right}}{4} \tag{2}$$

$$q = \frac{V_{BD} \cdot I_{tube}}{\pi d \overline{BD}} \tag{3}$$

The inner $T_{wall,i}$ is obtained from the outer wall temperature $T_{wall,o}$ by considering the analytical solution to the heat transfer phenomenon with the hypothesis of 1-D heat flux in the radial direction and uniform heat generation inside the tube, as shown in Equation (4):

$$T_{wall,i} = T_{wall,o,i} + \frac{V \cdot I}{4\pi\lambda_{tube} L_h} \cdot \frac{\left(\frac{D}{d}\right)^2 \cdot \left(1 - \log\left(\left(\frac{D}{d}\right)^2\right)\right) - 1}{\left(\frac{D}{d}\right)^2 - 1} \quad (4)$$

The saturation temperature $T_{sat,C}$ is a function of the local pressure value P_C and the latter is a function of the pressure drop ΔP_{tot} across the test section.

$$T_{sat} = f(P_C) = f\left(P_{in} - \frac{\overline{PC}}{L_h}\Delta P_{tot}\right) \quad (5)$$

The local vapor quality value is instead a function both of the local pressure value and the local enthalpy i_C:

$$x_C = f\,(P_C, i_C) \quad (6)$$

Finally, the local enthalpy is obtained by an energy balance considering the test section (subscript *TS*) and the preheater section (subscript *preh*), thus leading Equation (7):

$$i_C = i_{preh} + \frac{\dot{Q}_{preh}}{\dot{m}} + \frac{\dot{Q}_{TS} \cdot \left(\frac{\overline{AC}}{\overline{AE}}\right)}{\dot{m}} \quad (7)$$

All the transport and thermodynamic properties of the working fluid are calculated by the software Refprop 9.1 [18] whereas the data reduction is executed with a MATLAB [19] code.

3.2. Uncertainty analysis

The instrumental uncertainty was combined with the standard deviation of the measurement in the recording time. The law of propagation of error [20] was implemented for the derived parameters uncertainty using a coverage factor of 2, thus achieving a confidence level higher than 95%.

Table 2 reports the maximum uncertainty of the parameters of interest. For most of the database, the operating parameters' uncertainty is very low, whereas it becomes significantly higher if the dry-out occurrence is taken into account.

Table 2. Maximum uncertainty of parameters both considering and excluding dry-out conditions.

Parameter	Maximum uncertainty for 90% of the database	Maximum uncertainty for the whole database (including dry-out conditions)
Saturation temperature T_{sat}	±0.04 °C	±0.06 °C
Mass flux G	±7.6 %	±15 %
Heat flux q	±0.76 %	±1.3 %
Vapor quality x	±0.06	±0.07
Average heat transfer coefficient h_{mean}	±5.02 %	±30.4 %

4. Experimental results

4.1. Operating conditions and experimental procedure

All the experimental tests were carried-out in steady state conditions, with a record frequency of 1 Hz and in a recording time of 90 s. Specifically, the saturation temperature, mass flux and heat flux values were set by adjusting the demineralized water temperature through the thermostatic bath, by fixing the inverter frequency and regulating the electrical voltage of the DC power supply unit, respectively. Finally, the desired vapor quality value was regulated through the heat rate in the preheater section. In

the present study, the azeotropic mixture R513A has been studied by varying the saturation temperature from 20 to 50°C, mass flux from 150 and 300 kg/m^{2}s and imposed heat flux between 5 and 20 kW/m^2 in order to evaluate the effect of the operating parameters on the heat transfer coefficient.

4.2. Effect of the saturation temperature on the heat transfer coefficient

Figure 3 shows the effect of the saturation temperature on the average heat transfer coefficient as a function of the vapor quality for a fixed mass flux and heat flux values of 400 kg/m^{2}s and 20 kW/m^2, respectively. It can be noticed that the increase of the saturation temperature positively affects the heat transfer coefficient. In fact, the heat transfer coefficient increases from 7.8 kW/m^{2}K to 8.9 kW/m^{2}K (+14%) at a vapor quality of 0.3 and from 8.0 kW/m^{2}K to 9.4 kW/m^{2}K (+17.5%) at a vapor quality of 0.6 when the saturation temperature increases from 40°C to 50 °C. This can be explained by the increase of the nucleate boiling contribution probably due to the lower surface tension and consequently to the higher bubble growth.

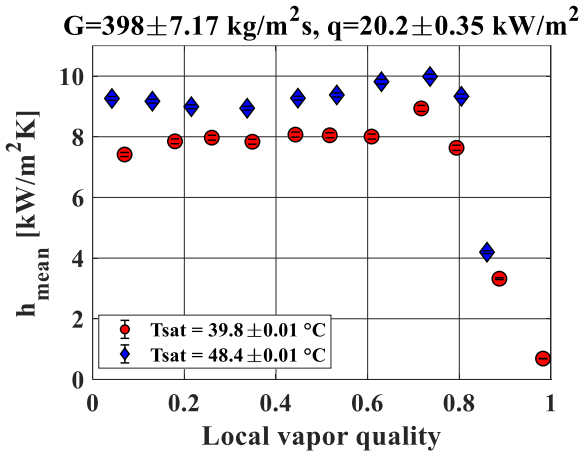

Figure 3. Heat transfer coefficient as a function of vapor quality. Effect of the saturation temperature for a mass flux of 400 kg/m^{2}s and a heat flux of 20 kW/m^2.

4.3. Effect of the mass flux on the heat transfer coefficient

The effect of the mass flux value on the heat transfer coefficient as a function of the vapor quality is reported in Figure 4 for a saturation temperature of 40 °C and a heat flux value of 10 kW/m^2 (Figure 4a) and a saturation temperature of 40°C and an imposed heat flux of 20 kW/m^2 (Figure 4b). The increase of the mass flux value positively affects the heat transfer coefficient. Particularly, for low mass flux value and relatively low imposed heat flux such as 150 kg/m^{2}s and 10 kW/m^2 the decreasing trend in the heat transfer coefficient is probably due to an anticipated dry-out phenomenon. As the mass flux value increases, the heat transfer coefficient is rather constant with the vapor quality due to the non-negligible convective heat transfer (see Figure 4a). For higher imposed heat flux values such as 20 kW/m^2, instead, the heat transfer coefficient seems to be not affected by the mass flux effect (see Figure 4b), implying that the nucleative boiling contribution plays a major role.

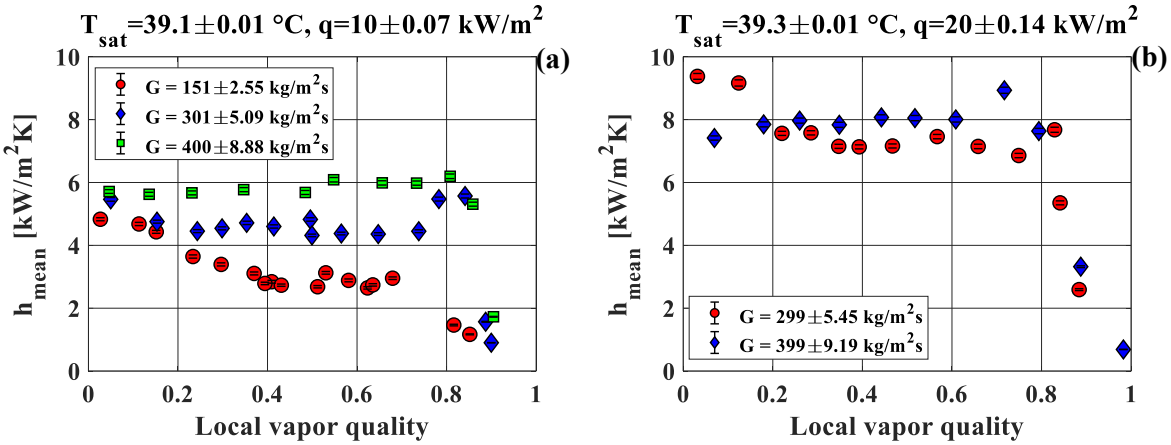

Figure 4. Heat transfer coefficient as a function of vapor quality. Effect of the mass flux for (a) a saturation temperature of 40 °C and a heat flux value of 10 kW/m^2 and (b) saturation temperature of 40 °C and heat flux value of 20 kW/m^2.

4.4. Effect of the heat flux on the heat transfer coefficient

Figure 5 exhibits the effect of the imposed heat flux as a function of the vapor quality for a fixed mass flux of 300 kg/m^{2}s and a saturation temperature of 40 °C. Particularly, at low vapor qualities the nucleate boiling contribution is stronger and the increasing in the heat flux significantly affects the heat transfer coefficient. In fact, it raises from 4.7 kW/m^{2}K for an imposed heat flux of 10 kW/m^2 to 9.1 kW/m^{2}K (+94%) for 20 kW/m^2 at a vapor quality value of 0.2. This behavior becomes less intense as the vapor quality increases: at a vapor quality of 0.6, the heat transfer coefficient passes from 4.3 kW/m^{2}K at a heat flux of 10 kW/m^2 to 7.1 kW/m^{2}K at 20 kW/m^2 (+65%). Finally, the vapor quality for dry-out inception is approximately equal to 0.83 and seems not to be greatly affected by the heat flux variation.

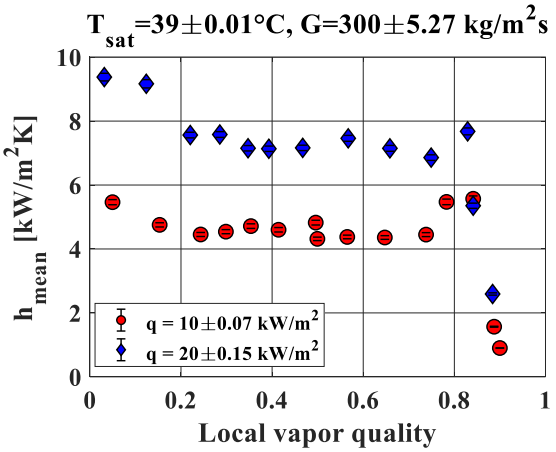

Figure 5. Heat transfer coefficient as a function of vapor quality. Effect of the heat flux for a saturation temperature of 40 °C and a mass flux value of 300 kg/m^{2}s.

4.5. Comparison of the heat transfer performance with R134a

The heat transfer performance of R513A has been compared with the one of pure R134a in the same operating conditions. Figures 6a-b show the effect of the working fluid for different mass flux and heat flux values. It is worth noting that, for low mass flux values, the effect of the working fluid is negligible (Figure 6a), probably due to the earlier dry-out phenomenon occurring in both cases, whereas R134a heat transfer coefficient is significantly higher as the mass and heat flux values increase (Figure 6b). In

fact, for a fixed vapor quality value of 0.5, the heat transfer coefficient of R513A is 7.1 kW/m^{2}K whereas the one of R134a is 11.2 kW/m^{2}K (+58%).

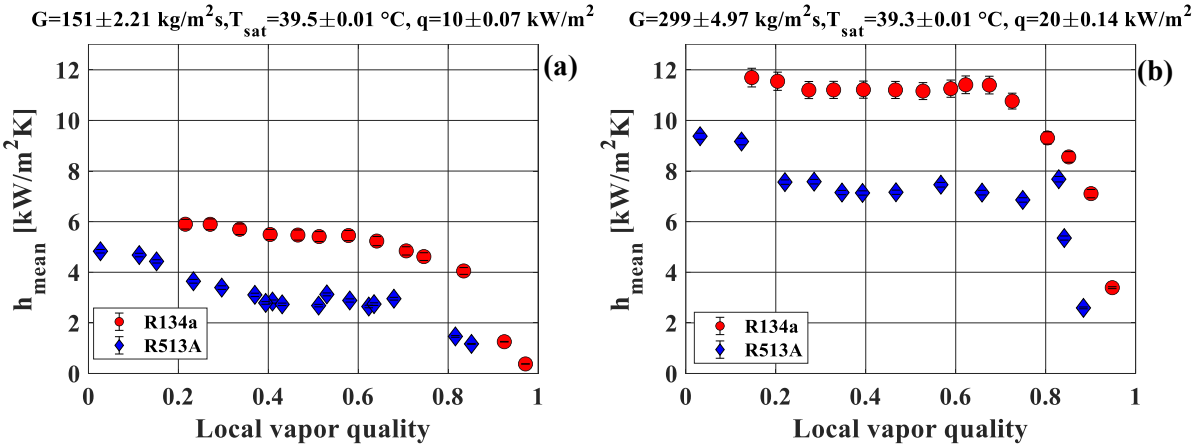

Figure 6. Heat transfer coefficient as a function of vapor quality. Effect of the working fluid (a) for mass flux value of 150 kg/m^{2}s, saturation temperature of 40 °C and heat flux of 10 kW/m^2 and (b) for mass flux of 300 kg/m^{2}s, saturation temperature of 40 °C and heat flux value of 20 kW/m^2.

5. Assessment of the existing prediction methods

Experimental data for both refrigerants R513A and R134a were compared to the predicted values from well-known correlations taken from literature in Figure 7a-b. The statistical analysis includes the Mean Absolute Percentage Error MAPE, the Mean Relative Percentage Error MRPE and the percentage of data points falling into an error range of ±30% ($\delta_{\pm 30\%}$). Two correlations have been chosen from the available ones thanks to their good agreement. Gungor-Winterton (1986) [21] method, developed for water and halogenated refrigerants, slightly underestimates R513A and R134a database (MRPE of -11.7% and -33.5%, respectively), with most of 60% of the R513A dataset falling into a range of error of ±30%. The modification of Gungor-Winterton [21] correlation proposed by Del Col (2010) [22] provides a slightly overestimation of R513A dataset (MRPE of 6%) and it shows a good agreement for the entire dataset, with most of 74% and 75% of the R513A and R134a points falling into an error range of ±30%, respectively.

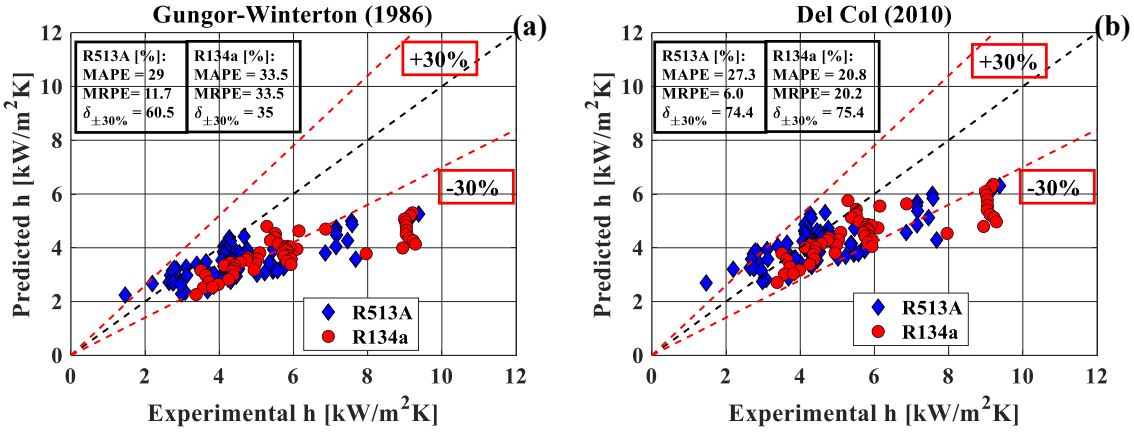

Figure 7. Predicted vs experimental heat transfer coefficient. (a) Gungor-Winterton (1986) method [21]; (b) Del Col (2010) correlation [22].

6. Conclusions

An experimental campaign for heat transfer coefficient data during flow boiling of R513A in a 6.00 mm single horizontal stainless-steel tube was carried-out. The main results are reported as follows:

- The mass flux and the heat flux positively affect the heat transfer coefficient trend. In particular, for low mass flux value such as 150 kg/m^{2}s and low imposed heat flux such as 10 kW/m^2, an anticipated dry-out occurs. As the mass flux increases, the heat transfer coefficient is relatively constant with the vapor quality value, probably due to the rise of the convective heat transfer. On the other hand, when the imposed heat flux is relatively high such as 20 kW/m^2, the heat transfer coefficient seems to be not affected by the increase of the mass flux value.
- The saturation temperature positively affects the heat transfer performance of R513A as well. For a mass flux value of 400 kg/m^{2}s and an imposed heat flux value of 20 kW/m^2, the percentage difference in the heat transfer coefficient reaches about 20% when the saturation temperature rises from 40 °C to 50 °C. This behaviour is probably due to the lower surface tension and consequently to the higher bubble formation, involving a higher nucleate boiling contribution.
- When compared to R134a refrigerant in the same operating conditions, the heat transfer coefficients of R513A are similar to those obtained with R134a during anticipated dry-out. The (negative) difference between them is significantly higher with the increasing of mass flux and heat flux values: at a mass flux of 300 kg/m^{2}s, saturation temperature of 40 °C and heat flux of 20 kW/m^2, the percentage difference reaches 60%.
- The assessment of two-phase heat transfer coefficient predictive methods has shown that Del Col correlation [22] provides the best agreement with the experimental data with more of 74% of the whole database falling into an error band of ±30% and a MAPE index equal to 27.3% (R513A) and 20.8% (R134a), respectively.

References

[1] Heath E 2017 *Int. Legal Mater* **56** 193-205
[2] The European Parliament and the Council of the European Union 2014 *Off. J. Eur. Union* **150** 195-230
[3] Citarella B, Viscito L, Mochizuki K, Mauro A W 2022 *En. Conv. Manag.* **253** 115152
[4] Sànchez D, Andreu-Nàcher A, Calleja-Anta D, Llopis R, Cabello R, 2022 *En. Conv. Manag.* **256** 115388
[5] Zheng H, Tian G, Zhao Y, Jin C, Ju F, Wang C 2022 *Case Stud. Th. Eng.* **36** 102203
[6] Mota-Babiloni A, Belman-Flores J M, Makhnatch P, Navarro-Esbrì J, Barroso-Maldonado J M 2018 *Energy* **162** 99-110
[7] Mota-Babiloni A, Navarro-Esbrì J, Pascual-Miralles V, Barragàn-Cervera A, Maiorino A 2019 *Appl. Therm. Eng* **147** 482-491
[8] Yang M, Zhang H, Meng Z, Qin Y 2019 *Appl. Therm. Eng* **146** 540-547
[9] Sun J, Li W, Cui B 2020 *Int. J. Refrigeration* **112** 348-356
[10] Longo G A, Mancin S, Righetti G, Zilio C 2019 *Int. J. Refrigeration* **108** 336-346
[11] Del Col D, Bortolin S, Torresin D, Cavallini A 2013 *Int. J. Refrigeration* **36** 353-362
[12] Mastrullo R, Mauro A W, Viscito L 2019 *Exp Th Fluid Sc* **105** 247-260
[13] Mauro A W, Napoli G, Pelella F, Viscito L 2020 *Int. J. Refrigeration* **119** 195-205
[14] Lillo G, Mastrullo R, Mauro A W, Pelella F, Viscito L 2019 *Appl Th Eng* 114146
[15] Diani A, Rossetto L 2019 *Int. J. Refrigeration* **107** 301-314
[16] Diani A, Rossetto L 2020 *Int. J. Heat Mass Transfer* **162** 120402
[17] Arcasi A, Mauro A W, Napoli G, Viscito L 2022 *Int. J. Heat Mass Transfer* **188** 122599
[18] Lemmon E W Mc Linden M O, Huber M L, 2009 *REFPROP NIST* Database **23**
[19] MATLAB 2019a Release, *Mathworks*
[20] Moffat J R 1985 *J. Fluids Eng.* **107** 173-178
[21] Gungor K, Winterton R 1986 *Int. J. Heat Mass Transfer* **29** 351-358
[22] Del Col D 2010 *Exp. Therm. Fluid Sci.* **34** 234-245